THE ROYAL SOCIETY

# High-resolution X-ray diffraction determination of composition grading in $Hg_{1-x}Mn_xTe$ grown by interdiffused multilayer organometallic vapour-phase epitaxy

By C. D. Moore† and B. K. Tanner

*Department of Physics, University of Durham, South Road, Durham DH1 3LE, UK*

The crystallographic structure of $Hg_{1-x}Mn_xTe$ grown on GaAs by an interdiffused multilayer organometallic vapour-phase epitaxial process has been investigated using high resolution X-ray diffraction. Most layers were almost 100% relaxed and of poor composition uniformity across the wafer. In contrast to layers grown by direct deposition of the ternary compound, no variation of double-axis rocking-curve width was found with thickness, but there was a linear variation with the Mn fraction. Triple-axis reciprocal space maps showed that a substantial gradient existed in the Mn composition with depth. This has been quantified by matching experimental data to simulations based on the Takagi–Taupin theory. Evidence has been found both for epitaxy and clumps of MnTe on the surface of samples with low $x$ content, providing a possible explanation of anomalous transport and magnetic phenomena.

**Keywords: high resolution X-ray diffraction; epitaxy; dilute magnetic semiconductor**

## 1. Introduction

Mercury manganese telluride, $Hg_{1-x}Mn_xTe$, is a dilute magnetic semiconductor (Furdyna 1988) which can be grown in the zincblende structure over a larger composition range than most II–VI ternary compounds. As HgTe is a semimetal and MnTe a semiconductor, varying the Mn fraction from 0 to 1 results in a band-gap range of −0.3–3.2 eV, thus giving potential for application in infrared detectors (Rogalski 1994). However, in contrast to the common infrared detector $Hg_{1-x}Cd_xTe$, the presence of strong exchange interactions results in an enhanced Zeeman splitting and Faraday rotation with further possibilities for use in magneto-optical isolators (Pain 1991). In this paper we demonstrate how currently available high-resolution X-ray diffraction hardware and software tools enable us to obtain a detailed understanding of the perfection of $Hg_{1-x}Mn_xTe$ layers grown by multilayer metal–organic vapour-phase epitaxy (MOVPE). We interpret these data in terms of accepted models of growth and relaxation in highly mismatched systems, relating the structure to a wider study of the electrical and magnetic properties (Horsfall *et al*. 1996).

† Present address: School of Engineering and Applied Science, University of California, Los Angeles, CA 90095-1595, USA.

## 2. Sample growth conditions

Epitaxial films of $Hg_{1-x}Mn_xTe$ were grown on (001) GaAs using an interdiffused multilayer process (IMP) following the method of Funaki *et al.* (1993*a*). The precursors used were di-isopropyl telluride (DIPTe), tricarbonyl methylcyclopentadienyl (TCMn), dimethylcadmium (DMCd) and dimethylzinc (DMZn). Elemental mercury was used in the growth of the HgTe components of the HgTe–MnTe multilayer formed prior to the interdiffusion which results in the ternary $Hg_{1-x}Mn_xTe$ layer. In all cases a 1 μm CdTe buffer layer was used to reduce the dislocation density in the $Hg_{1-x}Mn_xTe$ layer (Funaki *et al.* 1993*b*; Tatsuoka *et al.* 1994), an initial 0.1 μm ZnTe layer being needed on the GaAs substrate to ensure that the CdTe grew in the (001) orientation. DIPTe was used as a precursor instead of diethyl telluride as it permits growth at lower temperatures, reducing both outdiffusion from the substrate and stresses due to the differential contraction of substrate and layer on cooling. These conditions resulted in layers with thickness between a fraction of a micrometre and several micrometres and nominal compositions varying between 0 and 30% manganese.

## 3. X-ray optical technique

Double-axis high-resolution X-ray diffraction measurements were made in the laboratory using either the non-dispersive (+−) mode with a 004 reflection GaAs beam conditioner and Co-$K\alpha_1$ radiation, or a true monochromator consisting of a 022 four-bounce channel-cut silicon crystal followed by a 111 Ge crystal in the (++) geometry. Measurements in this latter geometry were undertaken using Cu-$K\alpha_1$ radiation. In both cases a beam area of *ca.* $1 \times 1\,mm^2$ was incident on the sample. Triple-axis measurements were made at station 2.3 of the SRS synchrotron radiation source at Daresbury Laboratory. The incident beam was monochromated by a water-cooled 111 channel-cut silicon crystal; all synchrotron radiation measurements were performed at a wavelength of 1.39 Å, which is close to the intensity maximum of the beamline. The analyser consisted of a 0.1 mm slit in front of the detector some 1 m from the specimen. A pure detector scan across the incident beam yielded an analyser resolution function which was Gaussian with full width at half height maximum (FWHM) of 45 arc seconds. The positions of the Bragg peaks from $Hg_{1-x}Mn_xTe$ and CdTe layers with respect to that from the GaAs substrate were used to determine the composition and relaxation of the layers. Hallam *et al.* (1993) showed that the FWHM of the double-axis and specimen-only (rocking-curve) triple-axis scan were dominated by mosaic tilts and so it was necessary to record the coupled $\theta$–$2\theta$ triple-axis scan in order to determine composition variation with depth. We note, however, that such scans are also sensitive to strain, and therefore it was essential to study initially the state of strain in the CdTe and $Hg_{1-x}Mn_xTe$ layers.

## 4. Results and discussion

### (*a*) *Relaxation in* CdTe *and* $Hg_{1-x}Mn_xTe$

Fully strained growth results in a tetragonal distortion of the layer and we can use measurements of symmetric and asymmetric Bragg reflections to determine the

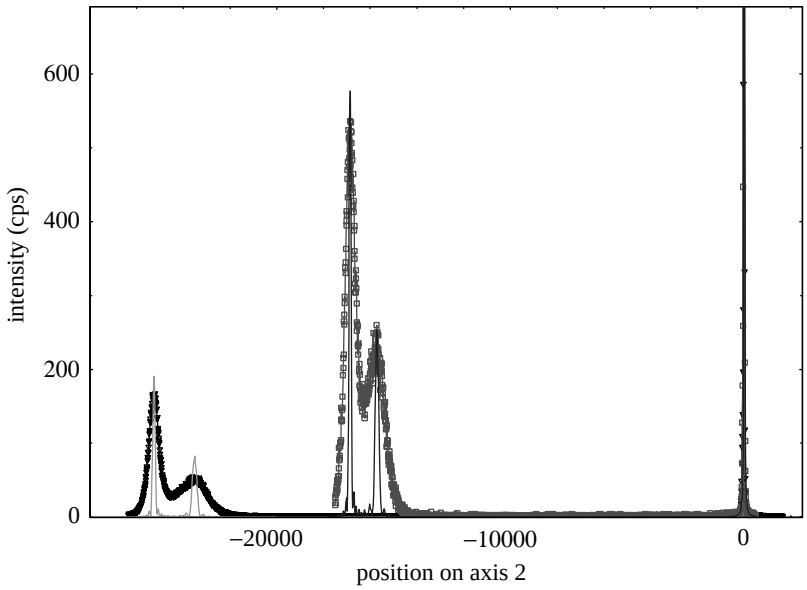


Figure 1. Superimposed 004 and 115 rocking curves for a typical layer (the 115 scan has been displaced to position the GaAs peak at the origin in both cases). Narrow peaks are those simulated using dynamical diffraction theory. The angular axis units are arc seconds.

degree of relaxation $R$, defined by

$$R = \frac{a_\mathrm{l} - a_0}{a_\mathrm{r} - a_0}, \tag{4.1}$$

where $a_\mathrm{l}$ is the in-plane layer lattice parameter, $a_0$ is the substrate lattice parameter and $a_\mathrm{r}$ is the bulk lattice parameter of a crystal of the same composition as that of the layer. A typical example of data for the symmetric 004 and asymmetric 115 reflections is shown in figure 1.

For each reflection, the peak to the far left is from CdTe, that from the $Hg_{1-x}Mn_xTe$ being adjacent on its right. Included in figure 1 are dynamical theory simulations using the Bede Scientific RADS code and we note the very substantial broadening of the layer peaks from those predicted for a perfect epitaxial layer. A 98.8% and 98.4% relaxation has been incorporated for the CdTe peak in the 004 and 115 reflections, respectively, resulting in good matching of the peak positions. Despite the broadening, these peak locations determine the relaxation to a precision of 0.05% and the difference between the two values arises from a small tilt of the epilayer with respect to the substrate. Data for the $1\bar{1}5$ reflection, where the specimen is rotated 90° about its surface normal, can also be fitted with a 98.4% relaxation, indicating that there is no significant asymmetry in the, almost complete, CdTe relaxation.

Using the Bede Scientific CAP software, which calculates the composition and relaxation of a ternary compound directly from the positions of the 004 and 115 peaks with respect to the substrate, we deduce $x = 0.29 \pm 0.1$ and $R = 99.3 \pm 1\%$ for the $Hg_{1-x}Mn_xTe$ layer. The simulated curves in figure 1 assume $x = 0.3$ and $R = 100\%$. By performing repeated rocking-curve measurements in a grid across the wafer, maps of composition were produced. Although previous high-resolution diffraction measurements on IMP samples had shown compositional gradients as low

as 0.03% $\mathrm{mm}^{-1}$ across the wafer surface (Hallam *et al.* 1995), the layers studied here had variations between 0.3 and 2.8% $\mathrm{mm}^{-1}$, comparable with those grown by direct alloy growth (DAG) (Tanner *et al.* 1993). The higher the Mn fraction, the higher was the variation in composition across the sample. However, in agreement with the earlier measurements on IMP samples, the fluctuation is almost random, there being no clear gradient along the gas-flow direction as is the case in the DAG layers. (Modelling of the DAG growth shows that the high gradient in this direction is almost inevitable due to the widely differing pyrolysis rates of TCMn and DIPTe (Sang *et al.* 1991).)

### (*b*) *Measurement of* $\mathrm{Hg}_{1-x}\mathrm{Mn}_x\mathrm{Te}$ *layer thickness*

The $\mathrm{Hg}_{1-x}\mathrm{Mn}_x\mathrm{Te}$ layer thickness was determined by measurement of the integrated intensity under the GaAs substrate peak compared with that from an uncoated GaAs wafer. As the X-rays diffracted by the substrate are far from the diffraction condition for the epilayers, the intensity is simply reduced by the normal absorption processes. Thus in the symmetric Bragg orientation

$$I_x/I_0 = \exp(-2\mu t/\sin\theta_\mathrm{B}), \tag{4.2}$$

where $I_x$ and $I_0$ are the diffracted and incident beams, respectively, $\theta_\mathrm{B}$ is the substrate Bragg angle and $\mu t = \sum \mu_i t_i$ is sum of the product of absorption coefficient and thickness for all the layers in the material. (As the absorption coefficient is dependent on the manganese fraction present, this must be first deduced from the peak positions and then included using the mass absorption coefficients weighted by the atomic fractions in calculation of the layer $\mu_i$ value.) In addition, as only the total $\mu t$ can be obtained by this technique we have to assume the constancy of the buffer layers at 1 μm CdTe and 0.1 μm ZnTe. Although the precision is relatively coarse, measurement of the integrated intensity of the CdTe peak confirmed this to be valid. All $\mathrm{Hg}_{1-x}\mathrm{Mn}_x\mathrm{Te}$ layers described had thickness varying between 0.5 and 2.5 μm, the level of variation across the wafer being typically 0.1 μm $\mathrm{mm}^{-1}$ and similar for all the samples except one. Where a clear gradient in thickness was observed, it was in the direction of gas flow, decreasing in thickness down the susceptor. This has been observed previously in IMP grown layers, and is attributed to the depletion of precursor partial pressures (Funaki *et al.* 1993*a*).

### (*c*) *Variation of* $\mathrm{Hg}_{1-x}\mathrm{Mn}_x\mathrm{Te}$ *peak FWHM with composition*

The most striking feature of the contour maps produced as a function of position across the wafer is the correlation between the manganese fraction and the FWHM of the $\mathrm{Hg}_{1-x}\mathrm{Mn}_x\mathrm{Te}$ peak. An example is shown in figure 2. Combining data taken from many positions off several samples reveals a linear relation between these parameters (figure 3) with an $x = 0$ intercept of 30 arc seconds, remarkably close to the theoretical FWHM for HgTe of 32 arc seconds.

As found in our previous studies of these highly mismatched II–VI compounds (Hallam *et al.* 1993), the double-axis rocking-curve width is comparable with that of the specimen-only (rocking-curve) scan in the triple-axis geometry with an analyser present. (In figure 3, we have included several data points from our triple-axis measurements and although these lie systematically below the double-axis line, the

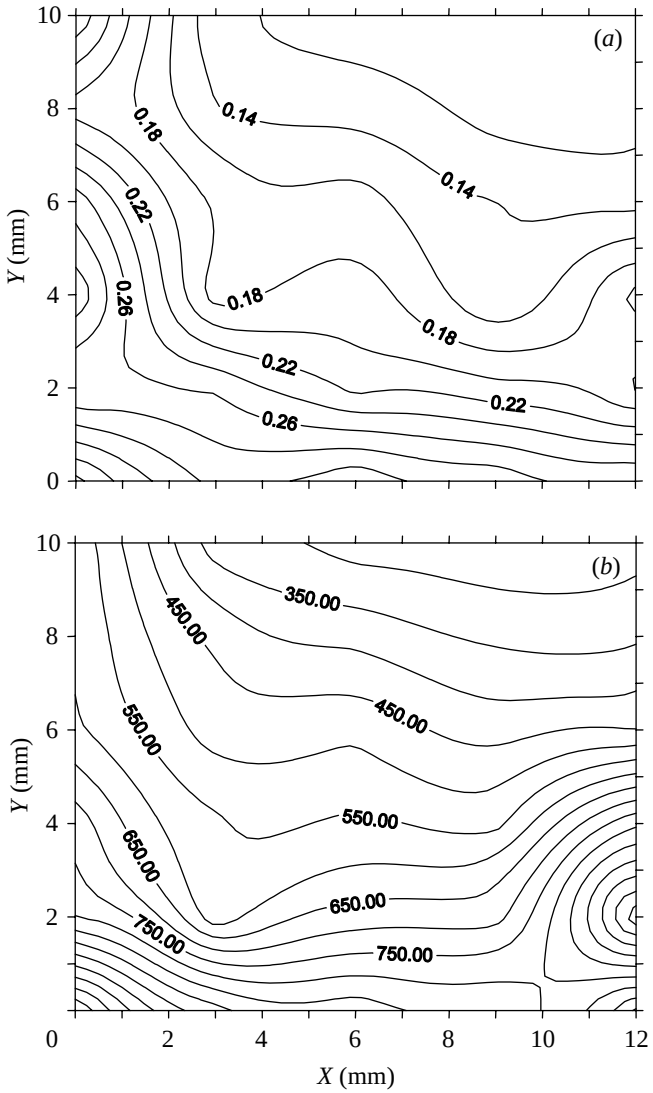


Figure 2. An example of the correspondence in variation of (*a*) Mn fraction and (*b*) FWHM in arc seconds of the $Hg_{1-x}Mn_xTe$ peak as a function of position across the wafer.

trend and magnitudes are similar.) Thus the variation cannot be associated with compositional variation as the triple-axis measurement is sensitive only to lattice tilts. We conclude that the dislocation density varies with Mn fraction.

Transmission electron microscopy investigations by Jones *et al*. (1996) into the presence and movement of point defects in IMP-grown $Hg_{1-x}Cd_xTe$, using a 4–6 μm CdTe buffer layer on GaAs, revealed that the microstructure obtained depended on $x$. With high $x$, small dislocation loops or precipitates were observed throughout the $Hg_{1-x}Cd_xTe$ layer, except close to the CdTe buffer. They concluded that dislocation loops formed during interdiffusion persist under high-$x$ conditions and this is consistent with the present data.

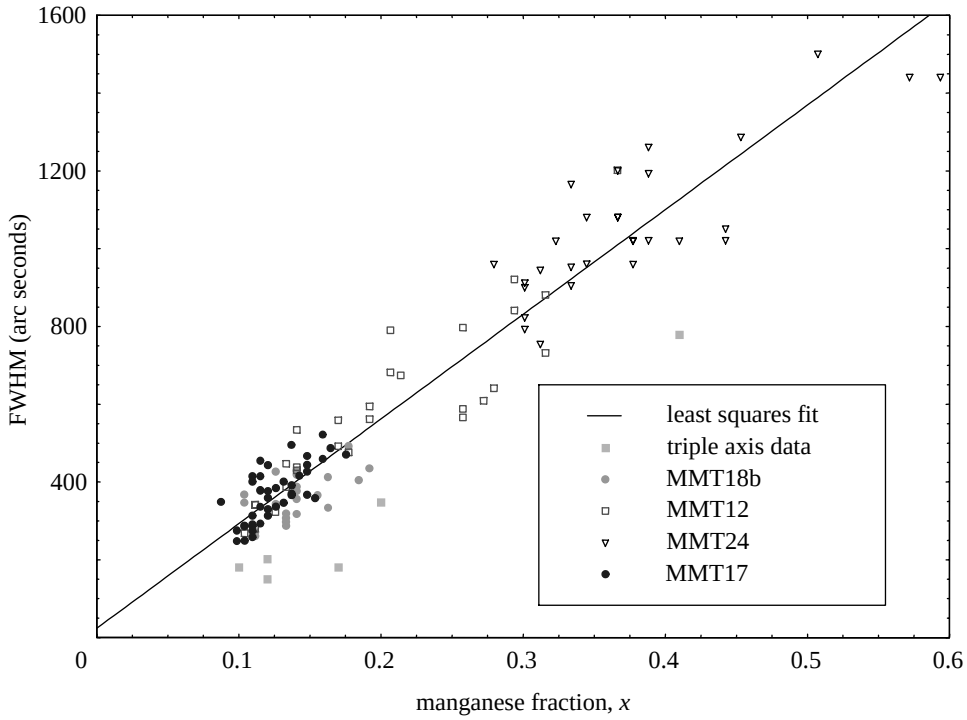


Figure 3. Relationship between Mn fraction and $Hg_{1-x}Mn_xTe$ peak FWHM.

### (*d*) *Variation of* $Hg_{1-x}Mn_xTe$ *peak FWHM with thickness*

The dependence of the FWHM on layer thickness in DAG $Hg_{1-x}Mn_xTe$ has been investigated by Hallam *et al*. (1993). When data were combined with that of Brown *et al*. (1989) for CdTe on GaAs, a linear relationship between FWHM and inverse thickness was obtained. No significant variations were found with Mn composition. Bernardi *et al*. (1991) have studied $Hg_{1-x}Cd_xTe$ grown by liquid phase epitaxy up to a thickness of 20 μm, and the graph of their FWHM against inverse thickness (although not plotted in the paper) also gives a good fit to a straight line. Ayers has developed a model, based on a half-loop mechanism for the annihilation of misfit dislocations, which predicts that the threading dislocation density in highly mismatched epilayers is proportional to $m/h$, where $m$ is the fractional lattice mismatch between substrate and layer and $h$ is the layer thickness (Ayers *et al*. 1991; Ayers 1994, 1995). Using a mosaic block model based on that of Gay *et al*. (1953), Koppensteiner *et al*. (1995) have shown that the threading dislocation density is directly proportional to the root-mean-square misorientation of the lattice planes in the layer. Double-axis X-ray topographs show that all the DAG layers consist of mosaic blocks of similar dimension and thus the inverse relation between rocking-curve FWHM and inverse thickness supports well the model of Ayers. The model also predicts correctly that the FWHM should be almost independent of Mn or Cd concentration. As the binary compound HgTe has a very large mismatch with GaAs, the small changes associated with differing Mn or Cd composition do not significantly affect the rocking-curve width.

In very marked contrast, except for the general observation that the thinner submicrometre IMP layers showed broader rocking curves than those from thicker layers, no systematic variation could be found between rocking-curve FWHM and thickness. The dominant variation was that with Mn composition (figure 3). Referring to the model of Koppensteiner *et al.* (1995), we see the implication is that the threading dislocation density is independent of thickness. We can understand such a constancy by recalling the growth mode, namely the deposition of multiple layers of HgTe and MnTe, these being of constant thickness with the total thickness determined by the number of repeats. Each binary layer is of sufficient thickness to relax totally with respect to the preceding layer by creation of new misfit dislocations at each interface, thereby preventing decrease in threading segments as the total layer thickness increases.

### (*e*) *Triple-axis reciprocal space maps*

Through a sequence of coupled specimen/detector $\theta$–$2\theta$ scans at different initial settings of the specimen, a map is built up of the scattering in reciprocal space. Examples of the scattering around the symmetric 004 and asymmetric 115 reciprocal lattice points recorded from a 6 μm thick layer are shown in figure 4. For a surface symmetric reflection, here the 004 reflection, the X-rays are only sensitive to lattice parameter variations normal to the surface. In the reciprocal space map of this symmetric reflection, the spread in intensity along $Q_z$ corresponds to a change in this lattice parameter, while a spread of scattering in the $Q_y$ direction corresponds to tilts in the lattice. In figure 4, on a logarithmic scale, the $Hg_{1-x}Mn_xTe$ peak shows a triangle-shaped distribution of intensity which has been observed frequently in II–VI semiconductors (Heinke *et al.* 1994*a*). The greatest diffuse scattering is seen around the peak position, which corresponds to a manganese fraction of 0.17. The diffuse scatter is symmetric about $Q_y = 0$, demonstrating a uniform tilt distribution. In contrast, the CdTe peak is symmetric in the $Q_z$ direction but is dominated by tilts; it is broader in $Q_y$ than in the $Q_z$ direction. The $Hg_{1-x}Mn_xTe$ peak is extremely sharp on the low $Q_z$ side; its position corresponds to a peak lattice parameter of 6.440 Å and a gradient towards lower lattice parameters. There are two possible explanations of this last feature. Firstly, the lattice parameter could be changing due to a strain gradient within the layer, i.e. a highly strained interface with a relaxed surface. Such gradients are seen in deliberately graded buffer layers in, for example, Si–Ge on Si or InGaAs on GaAs (Eldridge *et al.* 1995). Secondly, a gradient in Mn composition with depth through the layer could cause a broadening of the peak along $Q_z$ as a result of the change in lattice parameter of the changing composition ternary alloy. In this case, the broadening is towards a higher Mn fraction from that at the main peak. The extent of the diffuse scattering would decrease with less strain or higher $x$, yielding the triangle-like pattern in reciprocal space shown here. It is noteworthy that in the case reported by Eldridge *et al.* (1995), the interface is initially heavily relaxed, the layer growth subsequently becoming more coherent. The resulting broadening of the reciprocal space map is therefore inverted from the example here.

The broadening due to strain and compositional changes can be separated by the use of an asymmetric reflection, such as the 115 reflection shown in figure 4*b*, by measuring the angle between the surface normal and direction of intensity extension

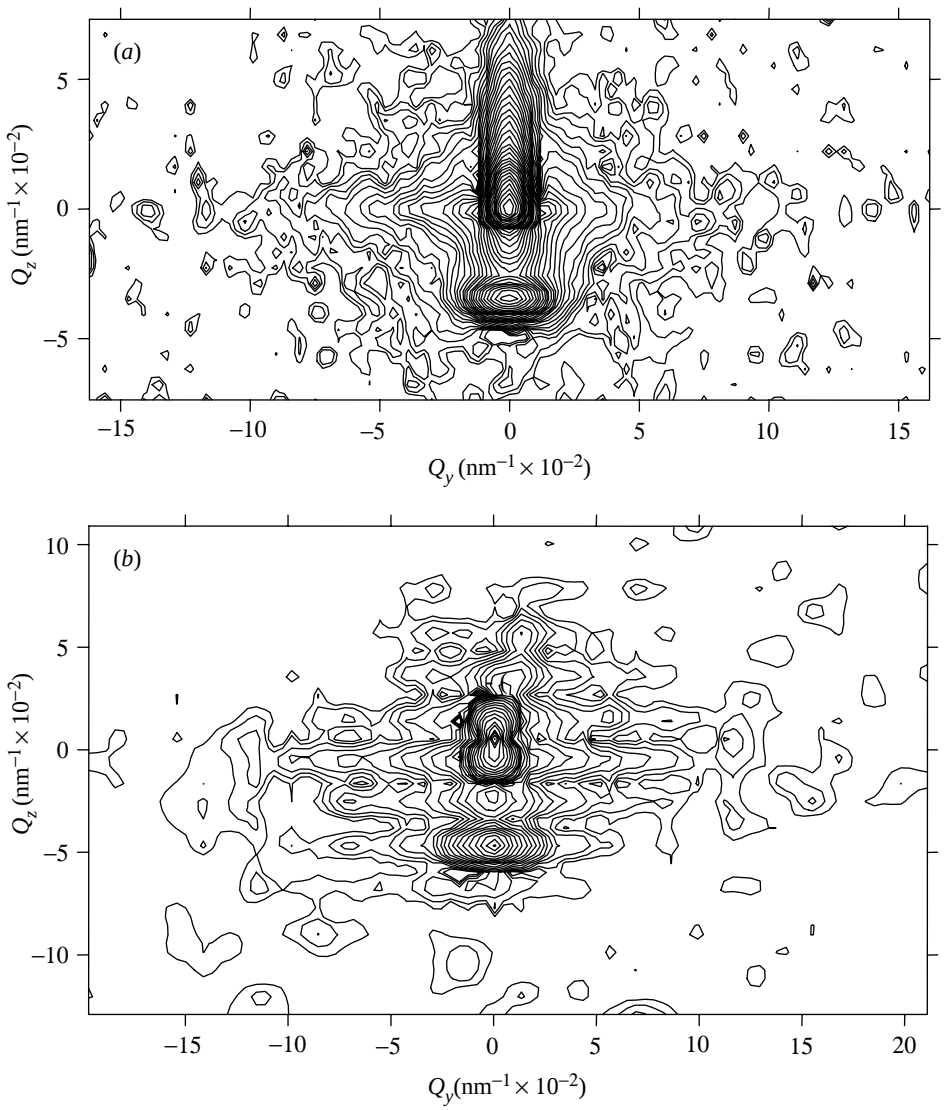


Figure 4. (*a*) Reciprocal space map around the 004 lattice point for a 6 μm layer. Upper peak is from the $Hg_{1-x}Mn_xTe$ and the lower peak from the CdTe. (*b*) Equivalent map around the 115 lattice point. (Note that in both figures, the $Q_z$-axis corresponds to the direction parallel to the diffraction vector.)

in reciprocal space. This is illustrated in figure 5 for both the symmetric and asymmetric cases. When, with respect to the substrate peak, the reciprocal lattice vector of the film lies along the line $\gamma = 1$, the direction normal to the surface, the layer is fully tetragonally strained. When it lies along $\gamma = 0$, the direction radial from the origin, it is fully relaxed and the layer is cubic. Heinke *et al.* (1994*a*, *b*, 1995) have developed a model for the separation of strain and compositional changes based on the so-called 'relaxation line'. Straightforward consideration of the transformation

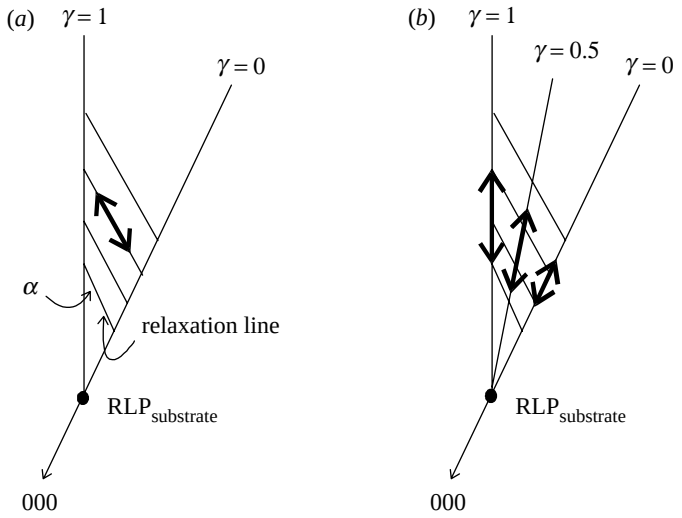


Figure 5. (*a*) Broadening in reciprocal space due to strain gradient and (*b*) concentration gradient.

between real and reciprocal space shows that the angle $\alpha$ at which the intensity extension lies with respect to $\gamma = 1$ is given by

$$\alpha = \arctan(D_i^{-1} \tan \varphi), \tag{4.3}$$

where $\varphi$ is the inclination angle of the lattice planes. $D_i$ is given by

$$D_i = -\varepsilon_\perp / \varepsilon_\parallel, \tag{4.4}$$

where $\varepsilon_\parallel$ and $\varepsilon_\perp$ are the in-plane and out-of-plane strains in the layer, respectively.

Thus the thick $Hg_{1-x}Mn_xTe$ layer shown in figure 4*b* is, as deduced from the double-axis rocking-curve simulations, fully relaxed and the lattice parameter variation arises from a compositional variation with depth. A symmetric pattern of diffuse scatter is seen in the 115 reflection, with the CdTe peak being dominated by tilts. There is less of a tail in the $Hg_{1-x}Mn_xTe$ peak, but the peak is itself again broader in the $Q_z$ direction than normal to it. The value of the peak position corresponds now to $x = 0.20$, but simple analysis of graded layers in this manner is not normally possible. As the asymmetric reflection is more surface sensitive than the symmetric reflection, the smaller extension of the peak indicates that the composition gradient is not constant, the steepest gradient being near the interface region. In contrast, an $Hg_{1-x}Mn_xTe$ layer less than 1 μm thick shows clear evidence of incomplete relaxation (figure 6). The layer is now sufficiently thin for the ZnTe buffer layer peak to be visible in the symmetric reflection (figure 6*a*) and simulation of the $\theta$–$2\theta$ scan (figure 6*b*) indicates that it is only 85% relaxed.

In the 115 reflection, the diffuse scatter is again extensive, but this time it is asymmetric about $Q_y = 0$. The CdTe peak is fairly symmetric but the $Hg_{1-x}Mn_xTe$ has two peaks, one that lies along $\gamma = 0$, and the other along $\gamma = 1$. The extended gradient above the $Hg_{1-x}Mn_xTe$ peak lies along the line corresponding to $\gamma = 0.77$. As the reciprocal lattice point is broadened along a direction that lies from the substrate peak along one of the $\gamma$ lines, we deduce that the layer is of constant $\gamma$,

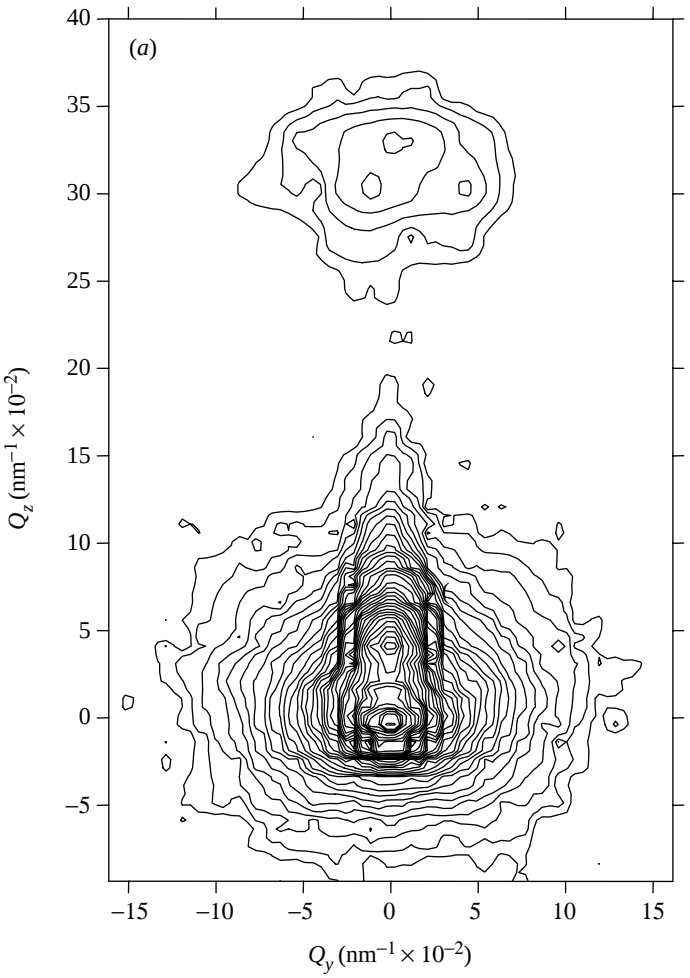


Figure 6. (*a*) Reciprocal space map around 004 for a submicrometre $Hg_{1-x}Mn_xTe$ layer. The broad peak at the top of the map arises from the ZnTe buffer layer.

i.e. relaxation, but with a composition varying with depth. As this is the thinnest layer produced for this study, and hence the one most likely to show strain effects, all the other layers can be assumed to have gradients in concentration only, and will be simulated as such.

### (*f*) *Depth dependence of* Mn *fraction*

The compositional variation as a function of depth in IMP-grown $Hg_{1-x}Cd_xTe$ layers has been studied by specular HeNe laser reflectance (Irvine *et al*. 1992), infrared transmittance spectra and secondary ion mass spectrometry (Shigenaka *et al*. 1992). Although the depth uniformity in II–VI IMP samples was found to be superior to that in DAG samples, some non-uniformity was observed in the case of MOVPE $Hg_xCd_{1-x}Te$/CdTe/ZnTe/GaAs (Irvine *et al*. 1992). In the IMP process, fluctuations in composition with depth must be linked either with instabilities in the growth period of one or both layers, or with the diffusion between layers occurring in a pref-

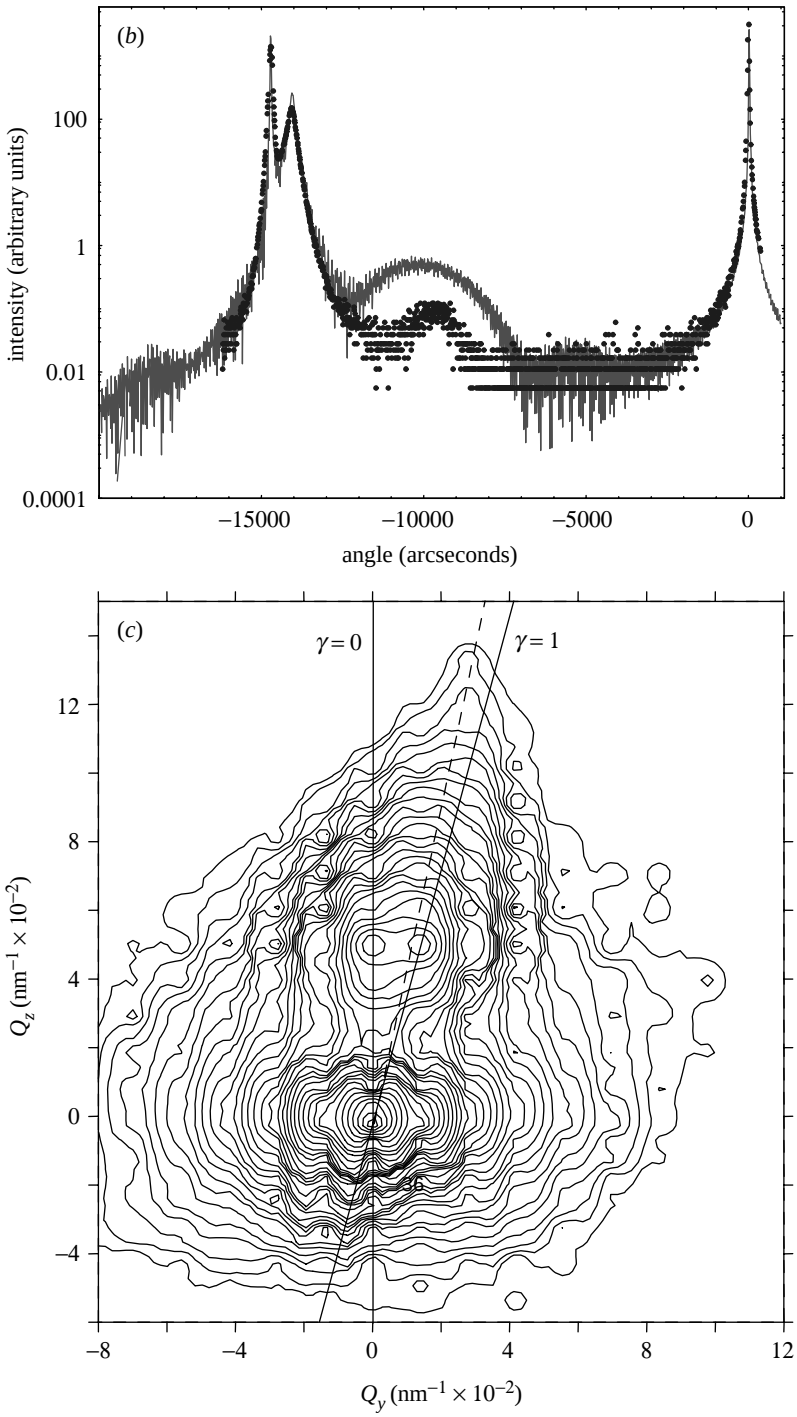


Figure 6. (*Cont.*) (*b*) Experiment and best-fit simulation of the 004 $\theta$–$2\theta$ scan. Solid line, simulation; points, experimental data. (*c*) Reciprocal space map around the 115 reciprocal lattice point.

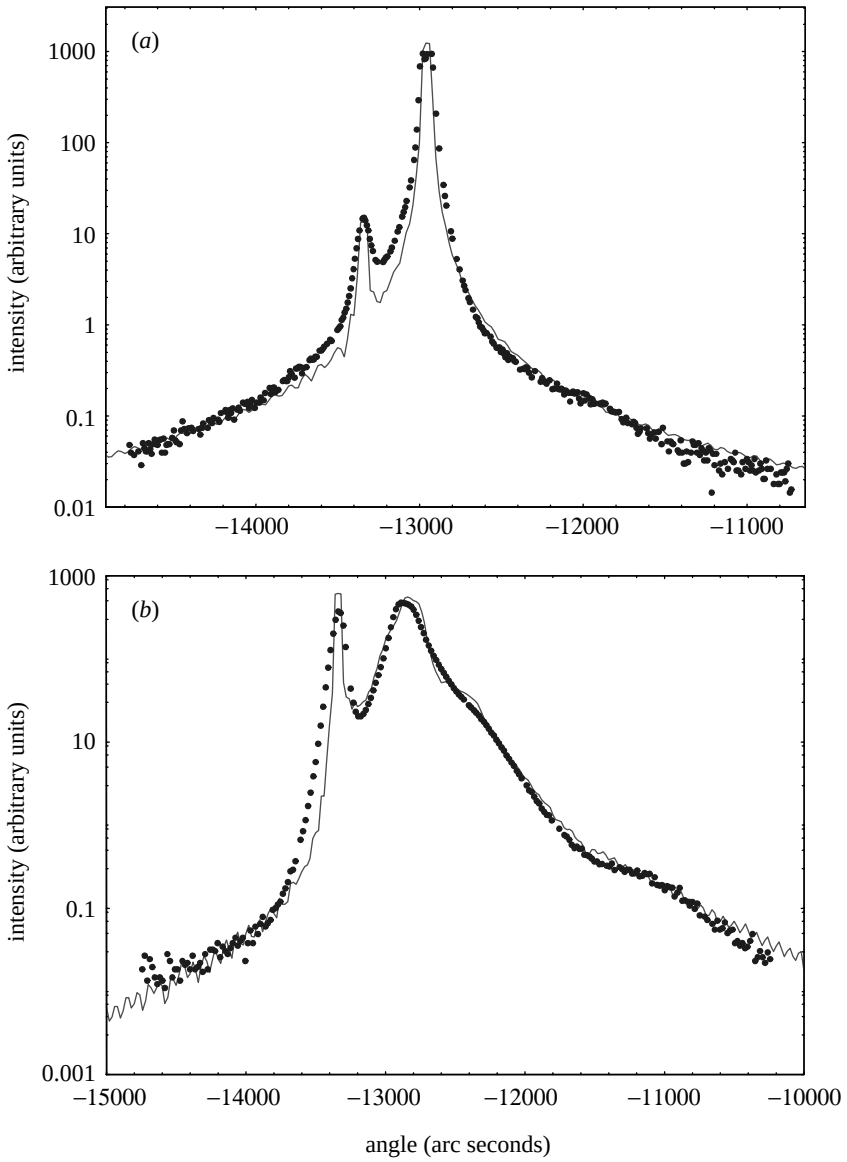


Figure 7. Experimental and simulated $\theta$–$2\theta$ scans for ($a$) a sample showing almost no compositional grading and ($b$) a severely graded layer: solid line, dynamical theory simulation; points, experimental data.

erential direction. If the former case applies, the uniformity should deteriorate with increasing thickness of the unstable layer. In order to determine quantitatively the magnitude and profile of the compositional grading, the experimental triple-axis $\theta$–$2\theta$ scans have been simulated using the Bede Scientific RADS code, which is based on the Takagi–Taupin formulation of the dynamical theory of X-ray diffraction. Figure 7$a$ shows a sample on which a great deal of transport and electrical data have been taken, as it is unusual in being n-type. The peaks are extremely narrow compared

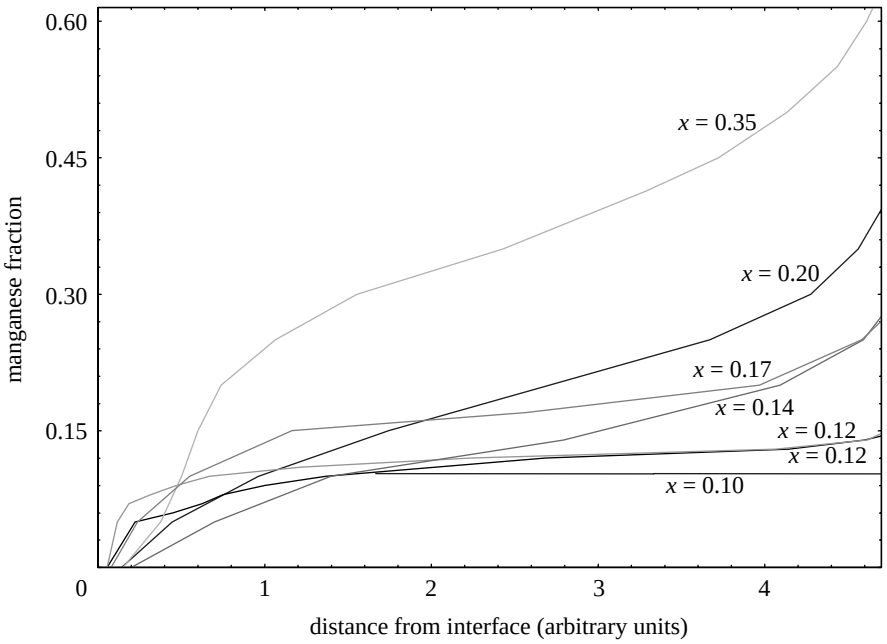


Figure 8. Mn concentration profile for layers of different composition.

with other samples (187″ for the CdTe, 161″ for the $Hg_{1-x}Mn_xTe$), and there is no evidence of grading. Good agreement is found between simulation and experiment, provided that the perfect crystal dynamical peaks are convolved with a function representing the strain distribution. A square function has been used here for simplicity. This convolution has little effect on the matching of the composition gradation which principally affects the tails of the rocking curve; only when plotted on a logarithmic scale is the effect obvious. The high intensity in between the two peaks compared with the simulation is probably due to some diffusion between the HgTe and CdTe layers, but the layer is predominantly of Mn composition $x = 0.103$.

In contrast, a scan and simulation displaying substantial grading is shown in figure 7*b*. The CdTe peak is still narrow, but the $Hg_{1-x}Mn_xTe$ peak shows asymmetric broadening. An additional low-intensity peak to the right of the plot has been simulated successfully as arising from cubic MnTe. This implies that the Mn has not fully diffused in this sample, leading to a low-Mn-content $Hg_{1-x}Mn_xTe$ layer, and probably discrete regions of MnTe.

Data for a whole series of layers of different composition have been fitted to simulations and the results are summarized in figure 8. For each lamella, the manganese fraction has been plotted at the central position, so the lines do not go through the origin. The total thickness of each layer has been scaled (to 5 μm), so the gradients of manganese with respect to depth can be compared. Data from the very top surface have been removed, due to the complication arising from the presence of small amounts of MnTe. As the peak fraction of Mn in the sample increases, so does the composition gradient. Only up to about $x = 0.12$ can uniform growth be maintained.

Irvine *et al*. (1992), in their studies of $Hg_xCd_{1-x}Te$/CdTe/ZnTe/GaAs attributed non-uniformity to changes in the DIPTe partial pressure (used for both CdTe and HgTe layers). This was due to condensation in the feed line, and was reduced by

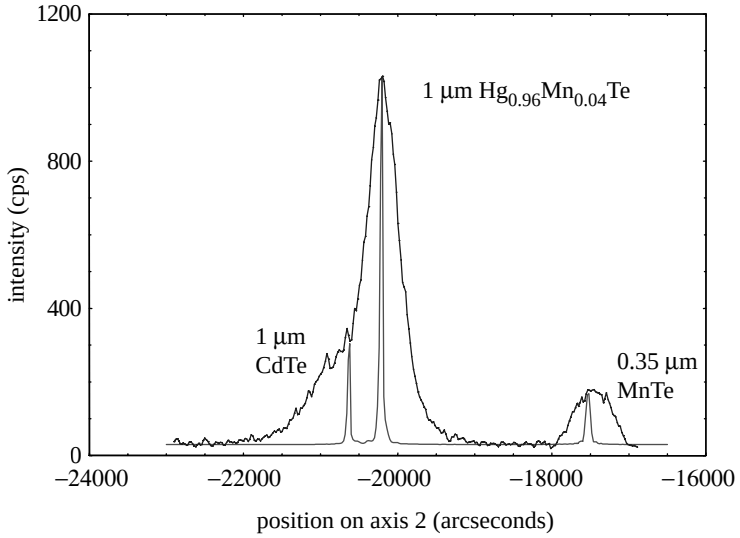


Figure 9. Double-axis rocking curve for a sample showing a clear MnTe peak. Sharp peaks correspond to those simulated using the dynamical theory with no defect broadening.

lowering the bubbler temperature. In the case of IMP-grown $Hg_{1-x}Mn_xTe$ (Funaki *et al.* 1993*a*), the room-temperature vapour pressure of TCMn is low, so the TCMn bubbler is heated to 75 °C to obtain sufficient precursor vapour pressure. This is high compared with the DIPTe bubbler temperature of 15 °C. The relationship between the amount of MnTe deposited and the non-uniformity suggests a similar explanation for the effect.

The presence of clumps of cubic MnTe was postulated by Horsfall (1997) to explain anomalous magnetic and magnetotransport behaviour in some samples. He observed saturation in Hall effect measurements and anomalies in the magnetoresistance, as well as evidence of magnetic ordering at room temperature. In some samples, there is evidence of epitaxial growth of an MnTe layer, for example in figure 9, where the experimental peaks occur at the positions corresponding to those simulated for relaxed layers of CdTe, $Hg_{1-x}Mn_xTe$ and MnTe. The scan of figure 9 is in the double-axis geometry with open detector, so the peaks are substantially broadened by lattice tilts. As for the sample in figure 7*b*, the Mn concentration is low, at $x = 0.04$. The MnTe peak was visible right across the sample surface, with an FWHM varying between 380 and 580″. The peak is far less evident through an analyser crystal, implying that the layer is highly tilted, and of poor crystallinity.

## 5. Conclusions

The crystallographic structure of $Hg_{1-x}Mn_xTe$ layers grown by an interdiffused multilayer MOVPE process has been investigated using a variety of high-resolution X-ray diffraction techniques. The variation in composition, thickness and perfection has been mapped across wafers showing that, despite improvement over direct alloy growth of the ternary compound, it remains difficult to produce layers of good uniformity with this growth technique. In the samples studied, the minimum compositional gradient was 0.3% Mn $mm^{-1}$. A correlation between crystal perfection and

manganese fraction was observed, and has been attributed to thin layers having higher Mn fraction, and the diffusion coefficient of precipitates varying with $x$, hence affecting the dislocation density.

Strain investigations have found the CdTe buffer layer to be 99%, and the $Hg_{1-x}Mn_xTe$ layer to be completely relaxed in all but the thinnest samples. The uniformity in composition perpendicular to the surface has been found to be poor, and simulations have been made of diffraction scans using a model of increasing Mn concentration towards the sample surface. Increased grading has been observed in high-$x$ samples. In addition, both epitaxial growth and clumps of MnTe have been identified on the surface of samples with low-$x$ content, so providing a possible explanation of anomalous transport and magnetic data.

Financial support from the Engineering and Physical Science Research Council is acknowledged. C.D.M. thanks Epitaxial Products International for support through a CASE studentship.

## References

Ayers, J. E. 1994 The measurement of threading dislocation densities in semiconductor crystals by X-ray diffraction. *J. Crystal Growth* **135**, 71–77.

Ayers, J. E. 1995 New model for the thickness and mismatch dependencies of threading dislocation densities in mismatched heteroepitaxial layers. *J. Appl. Phys.* **78**, 3724–3726.

Ayers, J. E., Ghandhi, S. K. & Schowalter, L. J. 1991 Threading dislocation densities in mismatched heteroepitaxial (001) semiconductors. *Mater. Res. Soc. Symp. Proc.* **209**, 661–666.

Bernardi, S., Bocchi, C., Ferrari, C., Franzosi, P. & Lazzarini, L. 1991 Structural characterization of $Hg_{0.78}Cd_{0.22}Te$/CdTe LPE heterostructures grown from Te solutions. *J. Crystal Growth* **113**, 53–60.

Brown, G. T., Keir, A. M., Gibbs, M. J., Giess, J., Irvine, S. J. C. & Astles, M. G. 1989 *Electrochem. Soc. Symp. Proc.* **89**, 171.

Eldridge, J. W., Matney, K. M., Goorsky, M. S., Chui, H. C. & Harris, J. S. 1995 Effect of substrate miscut on the structural properties of InGaAs linear graded buffer layers grown by molecular beam epitaxy on GaAs. *J. Vacuum Sci. Technol.* B **13**, 689–691.

Funaki, M., Hallam, T. D., Tanner, B. K. & Brinkman, A. W. 1993*a* Epitaxial growth of (Hg,Mn)Te by the interdiffused multilayer process. *Appl. Phys. Lett.* **62**, 2983–2985.

Funaki, M., Lewis, J. E., Hallam, T. D., Li, C. R., Halder, S. K., Brinkman, A. W. & Tanner, B. K. 1993*b* The MOVPE growth and characterization of $Hg_{1-x}Mn_xTe$. *Semicond. Sci. Technol.* **8**, S200–S204.

Furdyna, J. K. 1988 Diluted magnetic semiconductors. *J. Appl. Phys.* **64**, R29–R58.

Gay, P., Hirsch, P. B. & Kelly, A. 1953 *Acta. Metall.* **1**, 315.

Hallam, T. D., Halder, S. K., Hudson, J. M., Li, C. R., Funaki, M., Lewis, J. E., Brinkman, A. W. & Tanner, B. K. 1993 The characterization of epitaxial layers of the dilute magnetic semiconductor $Hg_{1-x}Mn_xTe$. *J. Phys.* D **26**, A161–A166.

Hallam, T. D., Oktik, S., Funaki, M., Moore, C., Brinkman, A. W., Durose, K. & Tanner, B. K. 1995 Uniformity in (HgMn)Te films grown by metal organic vapour phase epitaxy. *J. Crystal Growth* **146**, 604–609.

Heinke, H., Moller, M. O, Hommel, D. & Landwehr, G. 1994*a* Relaxation and mosaicity profiles in epitaxial layers studied by high resolution X-ray diffraction. *J. Crystal Growth* **135**, 41–52.

Heinke, H., Waag, A., Moller, M. O., Regnet, M. M. & Landwehr, G. 1994*b* Unusual strain in homoepitaxial CdTe(001) layers grown by molecular beam epitaxy. *J. Crystal Growth* **135**, 53–60.

Heinke, H., Eisfeldt, S., Kuhnheineich, B., Plahl, G., Moller, M. O. & Landwehr, G. 1995 Applications of the model of the relaxation line in reciprocal space in II–VI heterostructures. *J. Phys.* D **28**, A104–A108.

Horsfall, A. B. 1997 Characterization of epitaxial $Hg_{1-x}Mn_xTe$ films. PhD thesis, University of Durham.

Horsfall, A. B. Oktik, S., Terry, I. & Brinkman, A. W. 1996 Electrical measurements of $Hg_{1-x}Mn_xTe$ films grown by metalorganic vapour phase epitaxy. *J. Crystal Growth* **159**, 1085–1089.

Irvine, S. J. C., Bajaj, J. & Sankur, H. O. 1992 Complete *in situ* laser monitoring of MOCVD HgCdTe/CdTe/ZnTe growth on GaAs substrates. *J. Crystal Growth* **124**, 654–663.

Jones, I. P., Cheng, T. T., Aindow, M., Gough, J., Graham, A. & Gless, J. 1996 Precipitation and migration of point defects in MOCVD $Cd_xHg_{1-x}Te$. *J. Crystal Growth* **159**, 1096–1099.

Koppensteiner, E., Schuh, A., Bauer, G., Holý, V., Watson, G. P. & Fitzgerald, E. A. 1995 Determination of threading dislocation density in heteroepitaxial layers by diffuse X-ray scattering. *J. Phys.* D **28**, A114–A119.

Pain, G. N. 1991 Device application of $Hg_{1-x-y}Cd_xMn_yTe$ ($0 < x$, $y > 1$). In *Diluted magnetic semiconductors* (ed. M. Jain), pp. 563–585. Singapore: World Scientific.

Rogalski, A. 1994 Semiconductor infrared detectors. *Opt. Engng* **33**, 1392–1412.

Sang, W.-B., Durose, K., Brinkman, A. W. & Woods, J. 1991 *In-situ* mass-spectrometric investigation of tricarbonly (methylcyclopentadienyl) manganese (TCMN) pyrolysis mechanism during MOVPE. *J. Crystal Growth* **113**, 1–8.

Shigenaka, K., Uemoto, T., Sugiura, L., Ichizono, K., Hirahara, K., Kanno, T. & Saga, M. 1992 $Hg_{1-x}Cd_xTe$ epitaxial layers grown by low mercury partial-pressure metalorganic chemical vapour deposition and extended defect characterization. *J. Crystal Growth* **117**, 37–43.

Tanner, B. K., Hallam, T. D., Funaki, M. & Brinkman, A. W. 1993 High resolution X-ray diffraction of $Hg_{1-x}Mn_xTe$ epitaxial films. *Mater. Res. Soc. Symp. Proc.* **280**, 635–640.

Tatsuoka, H., Durose, K. & Funaki, M. 1994 Misfit dislocation arrangements in $(Hg_xMn_{1-x})Te$/CdTe and $(Hg_xMn_{1-x})Te$/CdZnTe heterostructures on (001), (111)B and (112)B substrates. *J. Crystal Growth* **145**, 589–595.